Two-photon ionization of H_2^+ by short laser pulses

A. Palacios,[1,*] S. Barmaki,[2] H. Bachau,[2,†] and F. Martín[1,‡]
[1]*Departamento de Química C-9, Universidad Autónoma de Madrid, 28049 Madrid, Spain*
[2]*Centre des Lasers Intenses et Applications (UMR 5107 du CNRS-CEA-Université de Bordeaux I), 351 Cours de la Libération, F-33405 Talence, France*
(Received 25 January 2005; published 17 June 2005)

We present a theoretical study of dissociative multiphoton ionization of the H_2^+ molecular ion in perturbative and nonperturbative regimes including both electronic and nuclear degrees of freedom. Differential (in proton and electron energy) ionization cross sections have been evaluated for various photon energies, laser intensities, and pulse lengths. We have found that the proton energy distribution is modulated by vertical Franck-Condon transitions but also by vibrational resonances associated with intermediate electronic states. We have also found that, as expected, nonperturbative results tend to the time-independent perturbative ones when both the pulse length increases and the laser intensity decreases. No divergence near intermediate-state resonances is found in the perturbative results when the nuclear motion is properly taken into account in the calculations.

DOI: 10.1103/PhysRevA.71.063405 PACS number(s): 33.80.Rv

I. INTRODUCTION

The rapid developments in laser technology have made recently available intense ultrashort laser pulses in the femtosecond (fs) and subfemtosecond (sub-fs) time regimes [1–3] which allow one to perform time-resolved spectroscopy at the atomic time scale [4,5]. Experiments based on high-order harmonic generation (HOHG) are now able to provide fs and sub-fs pulses in the xuv range (i.e., tens to hundreds of eV) with high enough intensity [6] to induce a nonlinear response of most atoms and molecules [7]. In addition, very recently, free electron lasers (FEL's) have also been able to provide xuv pulses in the fs regime [8,9]. The use of ultrashort xuv pulses opens up the way to study elementary two- and three-photon ionization processes in simple atoms (He,Ne,…) [7] and molecules (H_2^+,H_2,…). Simple systems that are accessible to accurate theoretical descriptions are crucial to guide theoretical developments in strong field multiphoton ionization and to reach a deeper insight on the basic mechanisms involved in the latter process.

The dynamics of bound electronic states typically occurs in the sub-fs time scale (the revolution time of an electron orbiting around a proton is $\sim$150 as). Electronic processes related to autoionization can be much slower and occur in the fs time scale. Recent experiments on rare gas atoms have taken advantage of this large difference and have led to interesting temporal pictures of ionization [4,10] and autoionization [5]. Molecular processes are even more interesting due to the presence of the nuclear motion, which is manifested through rotation, vibration, and the possibility of dissociation. Vibration and rotation typically occur in the fs time scale and, therefore, may compete efficiently with slow electronic processes such as autoionization [11]. The new available experimental techniques open up the possibility to analyze in detail the role of the nuclear motion in the xuv/fs and xuv/sub-fs context and, in particular, how this nuclear motion affects the ionization of molecules.

Although some theoretical work has been carried out for atoms interacting with xuv/fs and xuv/sub-fs laser pulses [12], applications to molecules are very scarce, mainly due to the complexity introduced by the nuclear degrees of freedom. Thus, many theoretical applications have concentrated on the simplest H_2^+ molecule. Detailed investigations of H_2^+ ionization have been carried out in the infrared (ir) regime (see [13] and references therein). Most of these applications have made use of one-dimensional (1D) models. A notable exception is the work of Ref. [14] in which the electronic motion is described by including the full dimensionality of the problem. For laser intensities of the order of 10^{13}–10^{14} W cm^{-2}, ionization is dominated by tunneling [13] in the ir regime, whereas it is dominated by multiphoton ionization in the xuv regime. This is because the ponderomotive energy is much larger in the former than in the latter case. In the xuv domain, multiphoton ionization of H_2^+ has been recently studied by solving the time-dependent Schrödinger equation (TDSE) within the frozen nuclei approximation (FNA) [15–17]. The effect of nuclear vibrations have been included in both perturbative [18] and nonperturbative [19] approaches.

The importance of nuclear motion in the study of resonance effects in H_2^+ ionization by xuv/fs and sub-fs pulses has been recently investigated [20]. Preliminary investigations have shown that, at variance with atoms, electronic resonance effects are barely seen in the photoelectron energy spectra. This is because the electronic resonances are diluted among the different dissociative states. In contrast, resonance effects are perfectly visible when one analyzes the kinetic energy distribution (KED) of the nuclear fragments.

The aim of the present work is to systematically investigate proton and electron energy distributions in two-photon

*Electronic address: alicia.palacios@uam.es
†Electronic address: bachau@celia.u-bordeaux1.fr
‡Electronic address: fernando.martin@uam.es

 ©2005 The American Physical Society

ionization of H_2^+ by xuv/fs and xuv/sub-fs laser pulses, both in perturbative and nonperturbative regimes, in the resonant and in the nonresonant regions. In particular, we would like to investigate the limits of validity of perturbation theory for both differential and integrated ionization rates. The advantage of using H_2^+ is that it allows one to treat the six dimensions of the problem within the Born-Oppenheimer (BO) approximation. Production of H_2^+ molecules in a well-defined vibrational state (e.g., $v=0$) is now possible and has in fact recently been used to study nonionizing dissociation dynamics [21] and tunneling ionization [22]. Previous attempts treating all dimensions of the problem have only been reported in the nonresonant region [19].

The paper is organized as follows. In Sec. II the theoretical methods used in the present work are explained in detail, in particular how the effect of the nuclear motion has been introduced both in the perturbative and nonperturbative regimes. All electronic and vibrational wave functions have been described in terms of *B*-spline basis sets. Computational details concerning the use of these basis sets are given in Sec. III. Section IV presents the different convergence tests that have been performed to select the electronic and nuclear basis sets. The results for differential as well as integrated two-photon ionization cross sections are presented in Sec. V. The paper ends with some conclusions in Sec. VI.

II. THEORY

A. Electronic and vibrational structure of H_2^+

We will neglect mass polarization terms and relativistic effects. Also, we will assume that there is no interaction between vibrational and rotational motions, so that the rotational wave function can be factored out. In the following, the origin of the electronic coordinates will be placed in the middle of the internuclear axis. The Hamiltonian of H_2^+ in the body-fixed frame can be written as the sum of the relative kinetic energy of the nuclei, $-\nabla_R^2/2\mu$, with μ the reduced mass, and the electronic Hamiltonian $H_{el}(\mathbf{r},R)$, which contains all the potential energy terms, including the nucleus-nucleus repulsion:

$$H(\mathbf{r},R) = -\frac{1}{2\mu}\nabla_R^2 + H_{el}(\mathbf{r},R). \tag{1}$$

The vector $\mathbf{r}$ indicates all electronic coordinates and R is the internuclear distance. In the BO approximation, the complete stationary wave function is given by

$$\Psi_{nv_n}(\mathbf{r},R) = \frac{\chi_{v_n}(R)}{R}\psi_n(\mathbf{r},R), \tag{2}$$

where the indices n and v_n indicate specific electronic and vibrational states. The electronic and nuclear wave functions are the solutions of

$$[H_{el} - \varepsilon_n(R)]\psi_n(\mathbf{r},R) = 0 \tag{3}$$

and

$$[T(R) + \varepsilon_n(R) - W_{nv_n}]\chi_{v_n}(R) = 0, \tag{4}$$

where $\varepsilon_n(R)$ is the BO potential energy curve of the nth electronic state, W_{nv_n} is the total energy of the molecule in the vibrational state v_n and the electronic state n, and

$$T(R) = -\frac{1}{2\mu}\frac{d^2}{dR^2} + \frac{J(J+1)}{2\mu R^2}, \tag{5}$$

with J the total angular momentum. As in previous works [11,23,24], the effect of the centrifugal term will not be taken into account because we are not interested in analyzing in detail rotational effects (in fact, we have found that ionization and dissociation patterns are practically independent of the value of J chosen to perform the calculations).

For a given value of R, the electronic continuum states of energy $\varepsilon_n(R)$ satisfy the usual boundary conditions corresponding to a single incoming (outgoing) spherical wave with a well-defined value of the angular momentum l and a combination of outgoing (incoming) spherical waves for all possible values of the angular momentum that are compatible with the molecular symmetry (see [24] for details). Formally, there are an infinite number of degenerate continuum states (one for each value of l) and, consequently, each of these states must be labeled using the two indices l, ε_n. As usual, these continuum states are normalized to the Dirac δ function (infinite norm), in contrast with bound electronic states that are normalized to the Kronecker δ function (finite norm). At variance with the electronic continuum, there is only a single vibrational continuum state for a given energy W_{nv_n}, which is due to our neglect of nuclear rotation and, therefore, of the coupling between different values of J. Vibrational states that belong to the continuum (i.e., dissociative states) satisfy normalization conditions similar to those of electronic states.

B. Perturbative approach

In this work we study two-photon ionization of H_2^+ from the $X\,^2\Sigma_g^+(1s\sigma_g)$ ground state using linearly polarized light. We restrict this study to the dipole approximation and to the case of H_2^+ molecules oriented along the polarization direction of the incident light. In this particular case, the dipole selection rule implies that $\Delta m=0$ and, therefore, that the first photon couples the initial molecular state to intermediate states of σ_u symmetry and the second photon couples the latter to final states of σ_g symmetry according to the sequence: $\sigma_g \rightarrow \sigma_u \rightarrow \sigma_g$.

Within the lowest order of perturbation theory (LOPT), the transition amplitude is given by

$$M^l_{fv_f gv_g} = \lim_{\epsilon\rightarrow 0}\sum_k \sum\!\!\!\!\!\!\int_{v_k} \frac{F^l_{fv_f,kv_k}F_{kv_k,gv_g}}{W_{kv_k} - W_{gv_g} - \omega + i\epsilon}, \tag{6}$$

where the indices f, k, and g refer to the final, intermediate, and ground electronic states, respectively. Vibrational states associated with these electronic states are denoted v_f, v_k, and v_g, respectively. The energy of the final state is determined by energy conservation, $W_{fv_f}=W_{gv_g}+2\omega$. The index f indi-

cates the energy of the electronic continuum state and l is the channel index (i.e., as explained above, the asymptotic value of the angular momentum). The integrals F_{kv_k,gv_g} and $F^l_{fv_f,kv_k}$ are given by

$$F_{kv_k,gv_g} = \int dR \chi_{v_k}(R)\chi_{v_g}(R)\langle \psi_k|D|\psi_g\rangle, \tag{7}$$

$$F^l_{fv_f,kv_k} = \int dR \chi_{v_f}(R)\chi_{v_k}(R)\langle \psi^l_f|D|\psi_k\rangle, \tag{8}$$

where the brackets indicate integration over electronic coordinates and D is the dipole operator.

At a given photon energy ω, the cross section, differential in the proton kinetic energy, can be written

$$\frac{d\sigma\ (\mathrm{cm}^4\ \mathrm{s})}{dE_{fv_f}} = C(2)\omega^{-2}\sum_l |M^l_{fv_fgv_g}|^2, \tag{9}$$

where $C(2)$ is a conversion factor from atomic to cgs units and is $2.505\,47\times10^{-52}$ cm^4 s, ω and $M^l_{fv_fgv_g}$ are given in a.u., and E_{fv_f} is the proton kinetic energy in the center of mass—i.e., $E_{fv_f}=W_{fv_f}-\varepsilon_f$ where ε_f is the energy of the ejected electron. The latter formula, which is the result of energy conservation in the photoabsorption process, shows that the cross-section differential in electron energy is simply the mirror image (referred to W_{fv_f}) of the cross-section differential in proton energy. A straightforward integration of Eq. (9) leads to the total cross section.

C. Nonperturbative approach: The time-dependent Schrödinger equation

In the nonperturbative regime, one directly solves the TDSE, which in the dipole approximation is written as

$$i\frac{\partial}{\partial t}\Phi(\mathbf{r},R,t) = [H + V(t)]\Phi(\mathbf{r},R,t), \tag{10}$$

where H is the Hamiltonian given in Eq. (1) and $V(t)$ is the laser-molecule interaction potential, which is written as the product $\mathbf{p}\cdot\mathbf{A}(t)$ in velocity gauge. In this gauge, for a total pulse duration T and a photon energy ω, the vector potential $\mathbf{A}(t)$, polarized along the vector $\mathbf{e}_z$ (the direction of the internuclear axis), is defined in the interval $[-T/2,+T/2]$ as

$$\mathbf{A}(t) = A_0 \cos^2\left(\frac{\pi}{T}t\right)\cos(\omega t)\mathbf{e}_z, \tag{11}$$

The vector potential is related to the electric field in length gauge:

$$\mathbf{E}(t) = -\frac{\partial}{\partial t}\mathbf{A}(t). \tag{12}$$

The time-dependent molecular wave function $\Phi(\mathbf{r},R,t)$ is expanded on the basis of stationary states $\Psi_{nv_n}(\mathbf{r},R)$ given in Eq. (2):

$$\Phi(\mathbf{r},R,t) = \sum_n \sum_{v_n} c_{nv_n}(t)\Psi_{nv_n}(\mathbf{r},R)\exp[-iW_{nv_n}t] + \sum_l \int d\varepsilon \sum_{v_\varepsilon} c^l_{\varepsilon v_\varepsilon}(t)\Psi^l_{\varepsilon v_\varepsilon}(\mathbf{r},R)\exp[-iW_{\varepsilon v_\varepsilon}t], \tag{13}$$

where the first term is a summation over bound electronic states (and their corresponding vibrational states, including the dissociation continuum) and the second one is an integral over electronic continuum states for all l (including again the corresponding vibrational states). Substituting this expansion in the TDSE and neglecting nonadiabatic couplings leads to a system of coupled differential equations that must be integrated over the whole pulse duration T to obtain the unknown coefficients c_{nv_n} and $c^l_{\varepsilon v_\varepsilon}$.

In the ionization channel, the differential density of probability in the proton kinetic energy is simply given by

$$\frac{dP}{dE_{\mathrm{H}^+}} = \sum_l \int d\varepsilon |c^l_{\varepsilon v_\varepsilon}(t = T/2)|^2, \tag{14}$$

where E_{H^+} is the center-of-mass energy of the outgoing protons. Similarly, the differential density of probability in the electron energy is given by

$$\frac{dP}{d\varepsilon} = \sum_l \sum_{v_\varepsilon} |c^l_{\varepsilon v_\varepsilon}(t = T/2)|^2. \tag{15}$$

Integrating Eq. (14) over vibrational energy [or Eq. (15) over ε] gives the total ionization probability P, which is related to the cross section σ:

$$\sigma\ (\mathrm{cm}^{2N}\ \mathrm{s}^{N-1}) = \left(\frac{\omega}{I}\right)^N \frac{C'(N)}{T}P, \tag{16}$$

where I is the laser intensity in W cm^{-2}, T is the pulse duration in seconds, ω is the photon energy in joules, and $C'(N)$ is the dimensionless coefficient taking into account the time dependence of the intensity, $C'(1)=\frac{8}{3}$, $C'(2)=\frac{128}{35}$, $C'(3)=\frac{3072}{693}$, …. Here T/C is an effective pulse duration [25] that takes into account the time dependence of the intensity. Thus, by including this term, we exclude the effect of having used a particular pulse shape and, therefore, the cross sections obtained from the TDSE approach will be directly comparable with those obtained from the time-independent LOPT approach.

III. COMPUTATIONAL METHODS

All electronic and vibrational wave functions are expanded on a basis of B-splines in a box of length $R_{\max}$. Due to the mass difference between electrons and protons, we define two different sets of B-splines to calculate the electronic and vibrational states (vibrational states are defined in a much smaller box than the electronic ones). The vibrational wave functions are expanded as

$$\chi_{v_n}(R) = \sum_{i=1}^{N} c_i^{v_n} B_i(R), \tag{17}$$

and the electronic wave functions of the ground (σ_g) and intermediate (σ_u) states are written using the one-center expansion:

$$\psi_n(\mathbf{r},R) = \sum_{l=0}^{l_{max}} \sum_{i=1}^{N_l} c_{il}^n \frac{B_i(r)}{r} Y_l^0(\mathbf{r}), \tag{18}$$

where the angular parts Y_l^0 are the spherical harmonics with $m=0$ (which is our case) and $l_{\max}$ is the maximum value of the angular momentum included in the expansion. As explained at length in [24,26], the advantage of the one-center expansion is that one avoids linear dependences in the basis set, but the price to pay is that, for large R, one must include large values of l to obtain a reasonable description of the cusp in the vicinity of the nuclei.

As the above wave functions are defined in a finite box, the resulting spectra are discrete. The eigenvalues that appear above the ionization limit when Eq. (3) is diagonalized correspond to the electronic continuum. Similarly, those lying above the dissociation limit when Eq. (4) is diagonalized correspond to vibrational continuum states. The corresponding continuum states are normalized to unity. Thus, to recover the correct normalization one must renormalize these states using the density of states. For example, in the case of the vibrational continuum, the continuum state with the correct normalization, χ_{v_n}, is related to the discretized continuum state that results from the diagonalization, $\tilde{\chi}_{v_n}$, through the formula

$$\chi_{v_n} = \rho_{v_n}^{1/2} \tilde{\chi}_{v_n}, \tag{19}$$

where ρ is the density of vibrational states given by $\rho_{v_n} = 2/(W_{n(v_n+1)} - W_{n(v_n-1)})$.

The final electronic continuum states (σ_g) are not obtained by direct diagonalization of the Hamiltonian in the above *B*-spline basis. As described in detail in [24], such a procedure does not lead to states with the proper asymptotic behavior. To avoid this problem we have used the L^2 close-coupling method introduced by Cortés and Martín [27] to describe the continuum states of atomic systems and later generalized in Refs. [27,28] to treat molecular continuum states. Thus, we define a set of orthogonal uncoupled-continuum states (UCS's) for each channel l:

$$\zeta_{\varepsilon_n l}(\mathbf{r}) = \sum_{i=1}^{N_l} c_i^n \frac{B_i(r)}{r} Y_l^0(\hat{r}), \tag{20}$$

where the index l denotes the angular momentum of the electron in the continuum and n indicates the electronic state of energy ε_n. Each UCS, for a given l, is formally associated with a projection operator P_l which satisfies

$$P_l \zeta_{\varepsilon_n l} = \zeta_{\varepsilon_n l},$$

$$P_l P_{l'} = \delta_{ll'} P_{l'}, \tag{21}$$

so that the UCS's are eigenfunctions of the uncoupled Hamiltonian:

$$\left(\sum_{l'} P_{l'} H_{el} P_{l'} - \varepsilon_n \right) \zeta_{\varepsilon_n l} = 0. \tag{22}$$

Solution of the latter equation in the finite box used to define the *B*-spline basis leads to discretized UCS's $\tilde{\zeta}_{nl}$ that are normalized to unity. Since, by definition, UCS's with different l's are not coupled, they can be renormalized exactly as if they were single-channel states—i.e., through the density of states $\rho_{nl}^{1/2}$:

$$\zeta_{\varepsilon_n l} = \rho_{nl}^{1/2}(\varepsilon_n) \tilde{\zeta}_{nl}, \tag{23}$$

where $\rho_{nl} = 2/(\varepsilon_{(n+1)} - \varepsilon_{(n-1)})$. Coupling between different l's is then introduced through the Lippman-Schwinger equation

$$\psi_{\varepsilon_n l} = \zeta_{\varepsilon_n l} + G^+(\varepsilon_n) V \zeta_{\varepsilon_n l}, \tag{24}$$

where $G^+(\varepsilon_n)$ is the Green function associated with the exact Hamiltonian H_{el} and

$$V = \sum_{\substack{ll' \\ l \neq l'}} P_l H_{el} P_{l'}. \tag{25}$$

This equation ensures that the resulting continuum state satisfies the proper boundary conditions. The Green function is evaluated as described in [27] using the basis of UCS's calculated in the previous steps. The method consists in projecting the usual relation $G^+ = G_0^+ + G_0^+ V G^+$, where G_0^+ is the Green function operator associated with the zero-order Hamiltonian given in Eq. (22), into the complete UCS basis and solving the resulting system of linear equations. For each value of R, the electronic states $\psi_{\varepsilon_n l}$ are evaluated in an energy grid (ε_n) that is chosen *a priori*. To ensure that, for each l, at least one of the UCS's corresponds to a chosen energy, we have used an inverse interpolation procedure [28], which consists in varying the box size until one of the ε_n eigenvalues coincides with the chosen energy. The energy grid is chosen to be equidistant in the vector k ($k = \sqrt{2\varepsilon_n}$) so that it simulates the spectrum that would be obtained in a box. As we will see below, this is important for coherence with the finite box used to solve the TDSE.

In all calculations presented below, the electronic states of H_2^+ have been represented in a basis of 140 *B*-splines of order $k=8$, including angular momentum from $l=0$ to $l=12$, in a box of radial length of 60 a.u. By changing the box size and/or the number of basis functions, we have checked that this basis set leads to practically converged energies in the Franck-Condon region. Figure 1 shows the potential energy curves of H_2^+ and a typical two-photon transition leading to ionization of H_2^+.

The *B*-spline basis sets used to describe the vibrational states are different in the LOPT and TDSE calculations, and will be described in the next section.

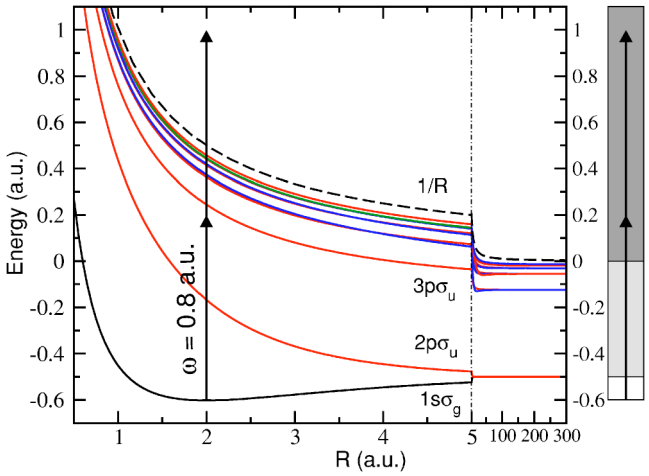

FIG. 1. Potential energy curves of H_2^+ as functions of internuclear distance. The figure shows the ground state, the ten lowest states of σ_u symmetry, and the ionization threshold $1/R$. A typical two-photon transition leading to ionization is illustrated by solid arrows. The two shadowed areas in the right-hand side column indicate dissociation and ionization+dissociation energy regions.

IV. CONVERGENCE TESTS

To analyze the quality of the basis sets and wave functions used in the present work, we have performed calculations in the fixed-nuclei approximation for $R=2.0$ a.u. (the equilibrium distance of H_2^+). This approximation has been already used by Apalategui *et al.* [18] to obtain two-photon ionization cross sections of H_2^+ using perturbation theory. A comparison between our results and those of Ref. [18] is given in Fig. 2. The agreement is excellent. We have checked that results obtained in the length and velocity gauges are practically undistinguishable. As usual, convergence of the calculated cross sections is much faster in the velocity gauge than in the length gauge. For this reason, all results presented below, both in the LOPT and TDSE frameworks, have been obtained in the velocity gauge.

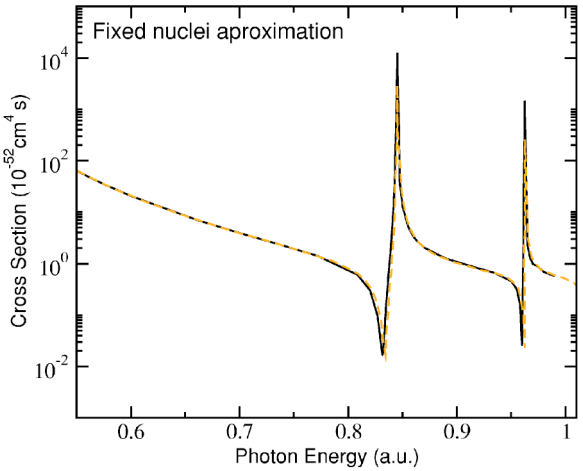

FIG. 2. Two-photon ionization cross section of H_2^+ as a function of photon energy. Results obtained within the fixed-nuclei approximation and the LOPT. Solid line: present results. Dashed line: results of Apalategui *et al.* [18].

As can be seen from the comparison of this figure with Fig. 1, perturbative calculations performed in the fixed-nuclei approximation lead to divergences when the photon energy exactly matches the energy difference between the ground state and a bound state of σ_u symmetry. This occurs because the denominator in Eq. (6) vanishes. This failure of LOPT is well known: similar divergences have been obtained in multiphoton ionization of atoms when the photon energy is in resonance with the energy required to excite those atoms (see, e.g., [12]). In the atomic case, this problem can be solved by including the laser-induced width of the intermediate states. However, as we will see later, a similar procedure cannot lead to a correct description of H_2^+ ionization in the resonance region. This failure in the LOPT calculations comes from the use of the fixed nuclei approximation and not from LOPT itself. This can be easily understood with the help of Fig. 1. The σ_u intermediate electronic states are repulsive and, therefore, support a continuum of vibrational states. Thus the situation is formally identical (although physically different) to above threshold ionization (ATI) in atoms: transitions associated with the first photon couple the ground state with a series of (vibrational) continuum states (see the shadowed areas in Fig. 1). In this case, the integral in Eq. (6) can be split into a principal value term and a δ function term representing a resonant one-photon transition to an intermediate continuum state (the pole). Contribution of this term is always finite and can be treated accurately with discretization techniques [26]. Consequently, two-photon ionization cross sections obtained within the LOPT should not diverge in the vicinity of intermediate-state resonances even without inclusion of the laser-induced width.

To account for the nuclear motion in LOPT, we have calculated the H_2^+ vibrational wave functions in a basis set of 400 B-splines of order $k=8$, contained in a box of 15 a.u. The initial vibrational state has $v_g=0$ and is supported by the $1s\sigma_g$ potential energy curve. All vibrational states v_k associated with a $k\sigma_u$ intermediate electronic state have been included in the calculations. At variance with results obtained in the fixed-nuclei approximation, we have found that, in the photon energy range considered in Fig. 2, convergence is already achieved by just including the lowest ten σ_u electronic states. This is because dipole matrix elements are strongly suppressed when the overlap between the initial and intermediate vibrational states is small, which is the case for the higher-σ_u states. Although this greatly simplifies the calculations, they still are computationally much more expensive than those obtained in the fixed-nuclei approximation.

The final states of σ_g symmetry have been determined for $l=0,2,\ldots$ on an energy grid between 0 and 1.5 a.u. that includes from 24 to 35 levels, depending on the photon energy. Obviously, the higher the photon energy, the higher the number of electronic states included. As mentioned above, evaluation of the pole contribution in Eq. (6) can be done within our discrete representation of the final states. Here we have used an approach proposed by Cormier and Lambropoulos [29] that explicitly avoids the evaluation of the limit by using a sufficiently small value of ϵ. The method is based on the following heuristic considerations. For a box of infinite size, the energy spacing between consecutive levels tends to zero and, therefore, evaluation of the transition amplitudes when ϵ

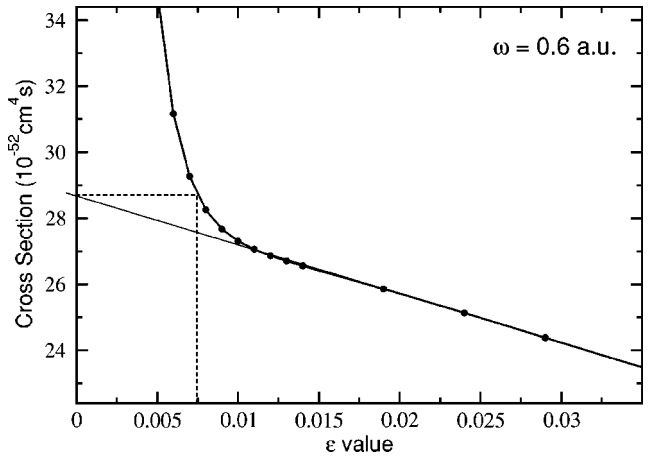

FIG. 3. Convergence of the two-photon ionization cross section of H_2^+ with ϵ [see Eq. (6)], for a photon energy of 0.6 a.u.

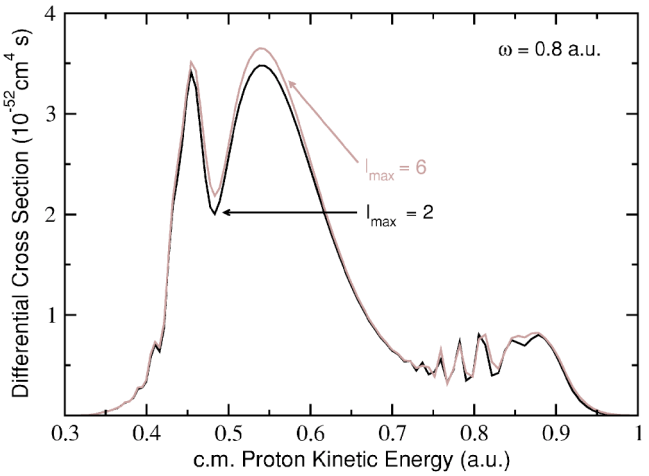

FIG. 4. Differential cross section for two-photon dissociative ionization of H_2^+ at a photon energy of 0.8 a.u. The proton kinetic energy is referred to the center of mass (c.m.) of the system. Results are shown for two different choices of l_{max} in the close-coupling expansion of the final electronic continuum states.

also tends to zero is meaningful. However, for a box of finite radial length, it is not possible to evaluate that limit because this would require the knowledge of the wave functions in energy intervals much smaller than those corresponding to that box. To avoid this problem the value of ϵ must be comparable to the energy spacing between consecutive energy levels. In Fig. 3 we show the variation of the two-photon ionization cross section with the value of ϵ chosen to evaluate Eq. (6). It can be seen that the cross section takes spurious values for very small values of ϵ, but for $\epsilon > 0.007$ a.u. it exhibits a simple monotonous behavior that allows one to easily extrapolate its value for $\epsilon = 0$. The value $\epsilon = 0.007$ is practically identical to the energy spacing between consecutive vibrational intermediate states. This value of ϵ has been used in all calculations reported below. We have checked that using ϵ values within the interval [0.005–0.009] barely changes the results. We have also checked that the results do not change when the size of both the nuclear and the electronic boxes are increased.

We have studied the convergence of the calculated cross sections with the number of partial waves included in the expansion of the final electronic continuum states. Figure 4 shows results obtained within the LOPT by including up to $l=6$ at a photon energy of 0.8 a.u.. The main contributions come from $l=0$ and $l=2$. In fact, the figure shows that very similar results are obtained by only including these two partial waves in the close-coupling expansion. The same conclusion is obtained at a photon energy of 0.6 a.u. Convergence of the TDSE calculations with l is similar. This is consistent with previous works performed at intensities of 10^{14} W/cm^2 using elliptic coordinates [17,19]. Therefore, in all LOPT and TDSE calculations reported below, we have only included the $l=0$ and $l=2$ channels in the final electronic states.

An important technical aspect in the TDSE calculations is the choice of the box size, which must be compatible with the pulse duration T. For such a pulse, the frequency spectra obtained from a Fourier transformation has a spectral width (half-height width) given by

$$\Delta\omega = \frac{2\pi}{T/2}. \tag{26}$$

To correctly treat the continuum spectra using a discretization procedure, the energy separation between discretized states (both vibrational and electronic states) must be smaller than the spectral width. This implies that the size of the electronic (nuclear) box must be chosen so that the condition $\Delta\varepsilon_n \ll \Delta\omega$ ($\Delta W_{n v_n} \ll \Delta\omega$) is fulfilled. This condition ensures that the electronic (vibrational) wave packet does not reach the limit of the electronic (vibrational) box before the end of the pulse. This technical constraint does not exist in LOPT because a basic assumption of this theory is that the pulse duration is sufficiently long ($T \to \infty$). Hence, the basis sets (i.e., the box lengths) used in LOPT are not necessarily the same as those used in the TDSE approach. In the TDSE calculations reported below, the electronic grid is chosen according to the pulse duration and the photon energy. For example, for a pulse duration of $T=10$ fs, an energy grid spacing of $\Delta\varepsilon < 0.03$ a.u. must be used, while for shorter pulses, one can use a larger energy spacing to simplify the calculations without a significant loss of accuracy. We have checked that several choices fulfilling the above criteria lead to TDSE results that are practically identical. To obtain the vibrational states used in the TDSE calculations, we have used a basis of 300 B-splines of order $k=8$ in a box of 14 a.u. for all pulse durations. Although the vibrational energy spacing obtained with this basis is not constant, it is always lower than 0.03 a.u. in the whole spectrum and, therefore, it is appropriate to describe the evolution of the system with pulses of 10 fs or shorter.

V. RESULTS AND DISCUSSION

We have solved the TDSE for various photon energies, laser intensities and pulse durations, and we have compared the results with those obtained with the LOPT. This allows us

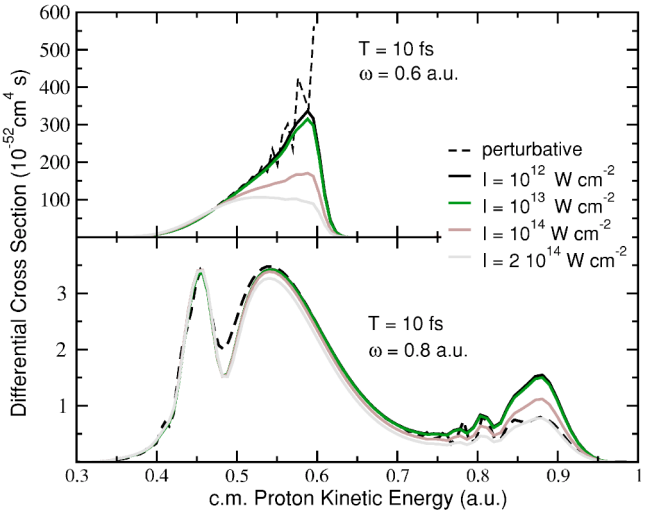

FIG. 5. Differential two-photon ionization cross sections of H_2^+ vs proton energy for different laser intensities and a fixed pulse duration of $T=10$ fs. The proton kinetic energy is referred to the center of mass (c.m.).

to establish the limits of validity for the latter, which is of practical interest due to its simplicity compared with the TDSE approach. We have chosen two different photon energies, $\omega=0.6$ and 0.8 a.u. In the first case, we are far from the region where intermediate-state resonances are expected to appear, while in the second case, we are close to the region where the first intermediate-state resonance appears in the fixed-nuclei approximation (see Fig. 2).

Figure 5 shows differential two-photon ionization cross sections for intensities ranging from 10^{12} to 2×10^{14} W cm^{-2} and a fixed pulse duration of $T=10$ fs. The figure also includes the results of the LOPT. As expected, the TDSE results tend to the LOPT ones as the laser intensity decreases. For $\omega=0.6$ a.u., the LOPT and TDSE results are close for $I\leqslant10^{13}$ W cm^{-2}. The perturbative approach is not appropriate when the intensity reaches 10^{14} W cm^{-2}. For $\omega=0.8$ a.u., similar patterns are observed, but there is a better agreement between TDSE and LOPT at larger intensities. We note in Fig. 5 that the cross section is much larger at $\omega=0.6$ a.u. than at $\omega=0.8$ a.u.

Figure 6 shows the final populations of the initial state, the dissociative ionization channels, and the dissociation channels (i.e., channels not leading to ionization) as functions of laser intensity. The populations in the dissociative and dissociative ionization channels are extracted from the solution of the TDSE by adding, at the end of the pulse, all contributions associated with individual dissociative and dissociative ionization states, respectively. The dissociation probability is much higher than the ionization probability for $I<10^{14}$ W cm^{-2}, whereas both probabilities are similar and even compete for larger intensities. This is consistent with the fact that, for photon energies ranging from 0.6 to 0.8 a.u., dissociation from the ground state is mainly due to one-photon absorption while ionization requires absorption of two photons. The log-log scale used in Fig. 6 shows that these populations are proportional to I and I^2, respectively, while the population of the ground state remains close to 1. This indicates that one- and two-photon absorption can be well described by perturbation theory, at least for $I<10^{14}$ W cm^{-2}.

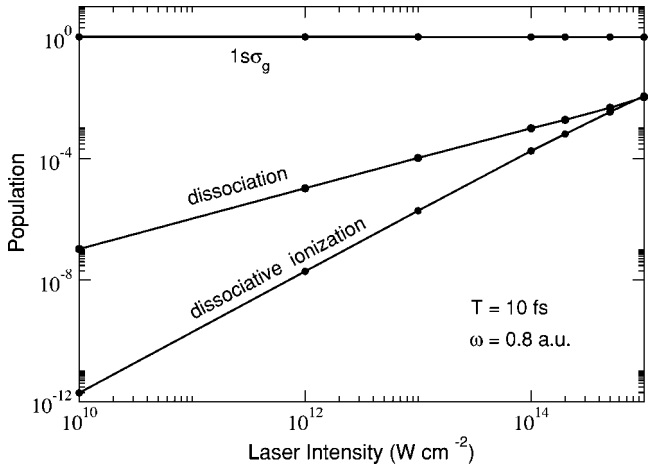

FIG. 6. Populations of the initial $1s\sigma_g$ state, dissociative and ionization channels of H_2^+ vs laser intensity. The laser parameters are indicated in the figure.

We analyze now the behavior of the differential two-photon ionization cross sections when the pulse duration is changed keeping a fixed intensity of $I=10^{12}$ W cm^{-2}. The results are shown in Fig. 7. As expected, TDSE results converge to the time-independent LOPT ones when the pulse duration increases. For long pulse duration (i.e., small bandwidth), peaks show up in the cross section. As we will discuss later, these peaks are related to virtual resonant transitions between electronic states. Most structures disappear for short pulses (i.e., large bandwidth) due to the larger energy spread of the pulse which makes resonant transitions to be less efficient. For the shortest pulses considered in this work

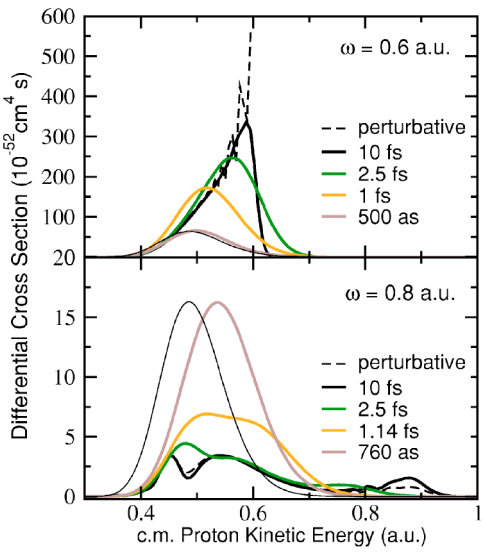

FIG. 7. Differential cross sections for different pulse durations at a fixed intensity of $I=10^{12}$ W cm^{-2}. The dashed line corresponds to LOPT results and the thin black line is the Franck-Condon factor between the initial $v_g=0$ and final vibrational states. This factor has been renormalized for a better comparison with the TDSE results.

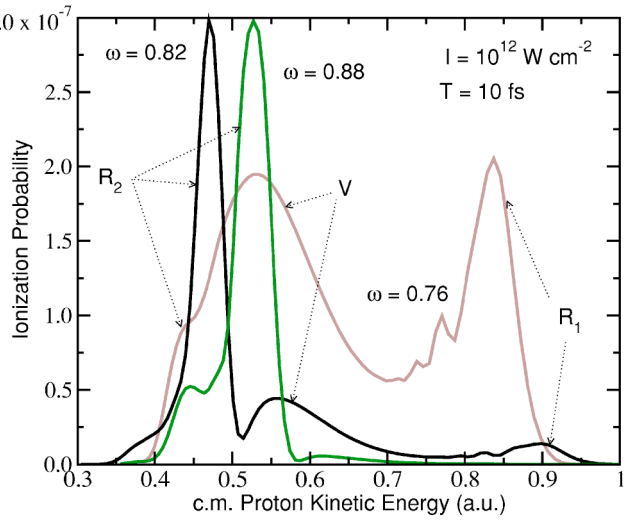

FIG. 8. Proton differential two-photon ionization cross sections of H_2^+ for three different photon energies. The different peaks are labeled R_1, R_2, and V, according to the notations used in Fig. 9 (see text).

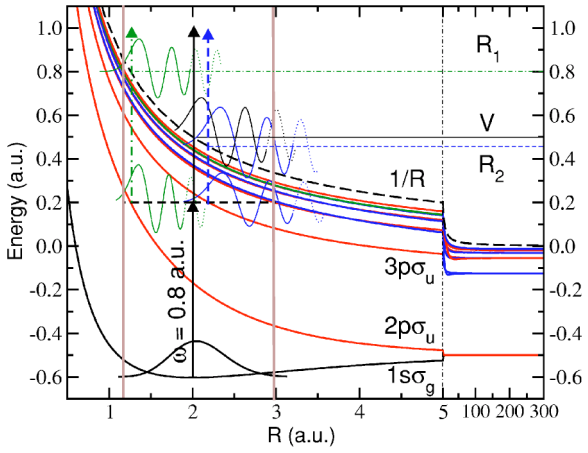

FIG. 9. A qualitative description of two-photon ionization using the potential energy curves of H_2^+. The figure shows the vibrational states of the resonant transitions that take place in the Franck-Condon region (limited by two vertical lines at $R\sim1$ and ~3 a.u.). Each transition is represented by an arrow. The crossing points between the upper three arrows and the $1/R$ curve correspond to different values of the proton kinetic energy (R_1, $R2$, and V).

(500 and 760 as), the differential cross section is almost proportional to the Franck-Condon factor between the initial and final vibrational states (see Fig. 7). Due to the dissociative character of the final state, this is almost equivalent to saying that it is proportional to the square of the initial vibrational state. A similar imaging of H_2^+ vibrational functions has been reported in reference [30] for ultrashort (5 fs) infrared pulses. In fact, when the pulse duration is much smaller than the vibrational time scale (which is above the fs), the differential cross section could be evaluated in the frozen nuclei approximation by calculating the ionization probability at different internuclear distances R, with a weight given by the Franck-Condon factor [17]. An ionization probability independent of the internuclear distance would give, in this approximation, a differential cross section matching perfectly the Franck-Condon behavior. The small differences between the Franck-Condon behavior and that observed for the shortest pulses are due to the slight dependence of the ionization rate with R.

We focus now our attention on the origin of the different peaks observed in the differential cross sections when the pulse duration is of the order of 10 fs or when the LOPT is used. In Fig. 8 we show the evolution of these peaks with photon energy in the range $\omega=0.76-0.88$ a.u. Since we are considering the case of long pulse duration, one can analyze the origin of the different peaks in terms of a two-photon transition consisting of (A) a "virtual" one-photon transition from the $^2\Sigma_g^+(v_g=0)$ ground state of H_2^+ to a $k\,^2\Sigma_u^+$ intermediate state in a narrow band of vibrational (continuum) states centered around v_k and (B) another transition from the latter intermediate states to the final $^2\Sigma_g^+$ ionization state in a vibrational (continuum) state v_f. These transitions are schematically represented in Fig. 9.

For $\omega\sim0.8$ a.u., transition (A) can connect the ground state with, in principle, any electronic intermediate state. This is because (i) the photon energy is larger than the energy separation between the ground state and the ionization energy at $R=\infty$ (see the right-hand column in Fig. 1) and (ii) all electronic intermediate states support a continuum of vibrational states so that the resonance condition is automatically satisfied. Nevertheless, among all intermediate states, only those with a large Franck-Condon (FC) factor will play a significant role. For $\omega\sim0.8$ a.u., these are the $^2\Sigma_u^+(2p\sigma_u)$ and the $^2\Sigma_u^+(3p\sigma_u)$ states, which are the only states lying inside the FC region at this photon energy (see Fig. 9). All other $k\,^2\Sigma_u^+$ states have negligible FC factors with the ground state. Therefore, transition (B) can only be efficient from one of these two states. The importance of this second transition depends on how large is the overlap between the intermediate and final vibrational functions. According to this FC picture, since the intermediate vibrational functions are most important near the classical turning points (CTP's), one can visualize transition (B) as a "vertical" transition from the CTP's of the active intermediate electronic states to the final ionizing state. This is illustrated in Fig. 9, which shows the two final states that can be efficiently populated: one with energy R_1 and the other one with energy R_2. This leads to peaks R_1 and R_2 shown in Fig. 8. Obviously, the position of these two peaks depends on photon energy because the position of the CTP's also does. For instance, diminishing ω shifts the CTP's to larger R (see Fig. 9). Thus, a vertical transition from the new CTP's leads to final vibrational states of lower energy and, therefore, to displacements of the R_1 and R_2 peaks to lower energy. This is precisely what is observed in Fig. 8.

Another mechanism is a direct two-photon transition from the initial $v_g=0$ vibrational state to the v_f vibrational states associated with the $1/R$ potential energy curve of H_2^+ (see Fig. 9). The corresponding FC overlaps have a maximum at ~0.5 a.u. and lead to the peak denoted V in Fig. 8. In contrast with peaks R_1 and R_2, the position of peak V does not vary with photon energy. This explains why this transition is observed even for pulses with a large bandwidth (see Fig. 7),

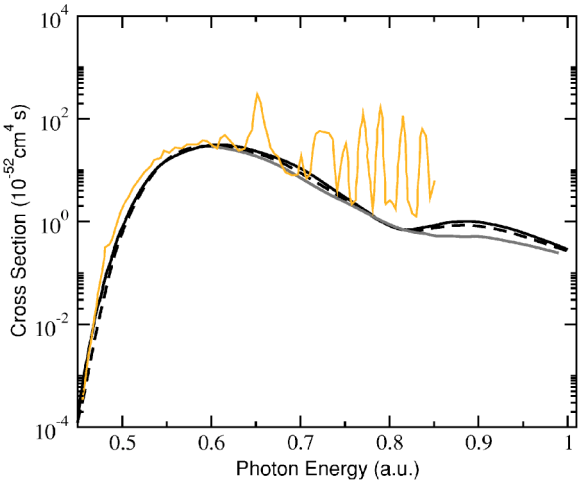

FIG. 10. Two-photon ionization cross section of H_2^+ as a function of photon energy. Black solid line: present TDSE results at $T=10$ fs and $I=10^{12}$ W cm^{-2}. Grey solid line: idem at $T=2.5$ fs and $I=10^{14}$ W cm^{-2}. Long dashed line: present LOPT results including the nuclear motion. Orange solid line: LOPT results from Apalategui *et al.* [18] including the nuclear motion in the reflection approximation.

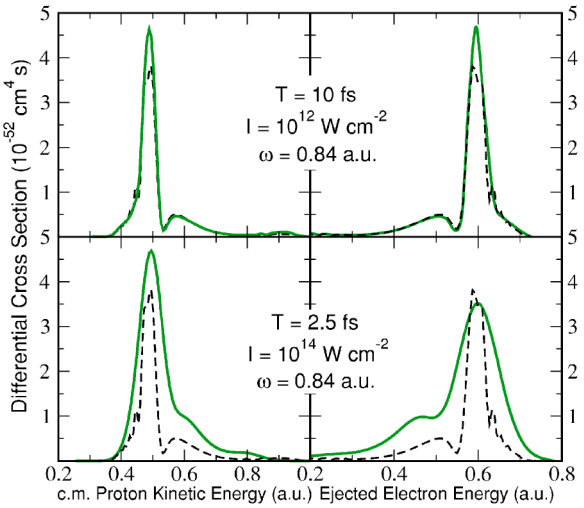

FIG. 11. Proton and electron differential cross sections corresponding to two-photon dissociative ionization of H_2^+. The photon energy is 0.84 a.u., in resonance with the $1s\sigma_g$-$3p\sigma_u$ transition. Solid (dashed) lines corresponds to TDSE (LOPT) results.

while transitions R_1 and R_2 can only be seen when the bandwidth is narrow.

It is easy to show that the positions of the different peaks contain the essential information about the potential energy curves of the intermediate electronic states of H_2^+ in the FC region. Indeed, for a given photon energy $\hbar\omega$, one can construct a one-to-one correspondence between the proton kinetic energies at the peak maximum, W_i, and the internuclear distance through the simple relation $R_i=1/W_i$ (in Fig. 9, these values of R correspond to the intersections of the R_1, R_2, and V horizontal lines with the ionization limit). Then one can relate each R_i value to a resonant one-photon transition from the ground state to an intermediate electronic state of energy $\varepsilon_k(R_i)=W_{gv_g}+\hbar\omega$. Thus, by varying the photon energy, one can obtain approximate potential energy curves $\varepsilon_k(R)$ for the relevant intermediate states [$^2\Sigma_u^+(2p\sigma_u)$ and $^2\Sigma_u^+(3p\sigma_u)$ in the present case]. We have checked that this procedure leads to potential energy curves in reasonable agreement with the ab initio ones.

We have also studied the variation of the total two-photon ionization cross section as a function of photon energy. This has been done within the TDSE approach for different intensities and pulse durations. The results are shown in Fig. 10. The figure also includes the results of the LOPT including the nuclear motion. The cross sections are very similar in all cases. A comparison of these results with those obtained in the LOPT+fixed nuclei approximation (see Fig. 2) shows clearly that the main effect of the nuclear motion is to dilute the intermediate-state resonances, which appear now as small oscillations in the cross sections. In particular, it is worth stressing that, as expected, no divergence is obtained when the nuclear motion is properly included in the LOPT (we recall that divergences within the LOPT are due to the use of the fixed nuclei approximation). For comparison we have also included in Fig. 10 the LOPT results of Apalategui *et al.* [18] that include the effect of the nuclear motion within the reflection approximation. It can be seen that their results are very close to ours for photon energies smaller than 0.6 a.u.; however, they exhibit unphysical oscillations at higher energies. This is due to the failure of the reflection approximation in the resonance region.

The similarity between the LOPT results and those obtained from the TDSE approach for pulse durations $T>10$ fs and intensities $I\leqslant 10^{12}$ W cm^{-2} are more evident if one compares electron and proton energy distributions. We show in Fig. 11 both distributions for a photon energy of 0.84 a.u. This energy is resonant with the $1s\sigma_g$-$3p\sigma_u$ transition and leads to a divergent cross section when the LOPT is applied in the framework of the fixed-nuclei approximation. For "long" pulse duration (10 fs, top of the figure) the proton and electron differential cross sections obtained with both LOPT and TDSE are similar. One can see that the proton distribution is the specular image of the electronic one, which is the consequence of energy conservation. The lower part of the figure shows the case of a smaller pulse duration (2.5 fs) and larger intensity (10^{14} W cm^{-2}). For reasons explained above, in this case the resonant transition is much less efficient and the proton distribution tends to the Franck-Condon one. In contrast, the electron distribution has now a width that is closer to the laser bandwidth (about 0.12 a.u.) and the specular behavior is lost. As in the case shown in Fig. 7, the distributions differ significantly from those obtained from the time-independent LOPT. Strictly speaking this does not mean that the perturbation theory does not work in general, because one could in fact use a time-dependent perturbation theory that integrates the temporal pulse shape, but it is much easier to directly use the TDSE.

VI. CONCLUSION

We have investigated two-photon ionization of H_2^+ in the photon energy range where this process is dominant over

single-photon ionization: $\omega=0.45-1.0$ a.u. We have used both perturbative (LOPT) and nonperturbative (TDSE) methods. In both cases, the theoretical approach includes the electronic and nuclear motions within the Born-Oppenheimer approximation. When the fixed nuclei approximation is used, the total two-photon ionization cross sections exhibit sharp resonances associated with intermediate electronic state. In contrast, when the nuclear motion is included, the total cross section does not exhibit pronounced resonances: they are only observed when the kinetic energy of the ejected protons is analyzed. The two-photon ionization cross sections calculated within the TDSE and (time-independent) LOPT approaches are very similar for a wide range of intensities ($<10^{14}$ W cm^{-2}) and pulse durations (>2.5 fs). As expected, for larger intensities and shorter pulses, the LOPT does not work.

The calculated proton kinetic energy distribution varies dramatically when the pulse duration goes from the femtosecond regime to the subfemtosecond regime (in which the pulse duration is smaller than the vibrational time scale, which is of the order of the femtosecond). For pulses of the order of 1 fs or less, the proton kinetic energy distribution closely follows the shape of the Franck-Condon factor between the $v_g=0$ initial state and the final dissociative states (which is quite similar to the behavior observed in one-photon ionization). The electron distribution shows a broader structure, reflecting the laser bandwidth. When the pulse duration approaches 10 fs, the proton and electron energy distributions show peak structures (one specular of the other) associated with two "virtual" one-photon resonant transitions involving intermediate vibronic states. Such structures are absent in one-photon ionization.

The pulse durations and wavelengths investigated in this work are currently produced in many laboratories. Thus, two-photon ionization experiments in which the ion energy distribution is analyzed can be envisaged in the short term. In this respect, the simple model proposed in this paper will allow one to easily interpret the origin of the different peaks observed in the kinetic energy distribution. This leads to an even more interesting possibility: the use of the proton energy distribution observed in two-photon ionization experiments as a probe of the pulse characteristics (duration and wavelength) in the femtosecond and subfemtosecond domains. Besides H_2^+, one could also consider D_2^+, which can be handled more easily in experiments. In this case, the vibrational period is ~ 20 fs, which would allow one to explore a slightly different time regime.

Finally, it is worth stressing that, although we have focused on a specific pulse envelop, similar conclusions are expected for other pulse envelops having similar duration and comparable shape. Variations with the pulse envelop have been recently predicted ([31] and references therein), but only for pulses that strongly differ in shape (e.g., for symmetric and asymmetric pulses). The possibility of similar effects in the present context should be the subject of future work.

ACKNOWLEDGMENTS

Work supported by the DGI (Spain) Project No. BFM2003-00194 and the European COST action D26/0002/02. We thank the CCC-UAM (Madrid, Spain) and the CINES (Montpellier, France) for computer time.

[1] M. Drescher, M. Hentschel, R. Kienberger, G. Tempea, C. Spielmann, G. A. Reider, P. B. Corkum, and F. Krausz, Science **291**, 1923 (2001).
[2] A. Baltuska, Th. Udem, M. Uiberacker, M. Hentschel, E. Goulielmakis, Ch. Gohle, R. Holzwarth, V. S. Yakovlev, A. Scrinzi, T. W. Hänsch, and F. Krausz, Nature (London) **421**, 611 (2003).
[3] P. Agostini and L. F. DiMauro, Rep. Prog. Phys. **67**, 813 (2004).
[4] R. Klenberger, E. Goulielmakis, M. Uiberacker, A. Baltuska, V. Yakovlev, F. Bammer, A. Scrinzi, Th. Westerwalbesloh, U. Kleineberg, U. Heinzmann, M. Drescher, and F. Krausz, Nature (London) **427**, 817 (2004).
[5] M. Drescher, M. Hentschel, R. Kienberger, M. Uiberacker, V. Yakovlev, A. Scrinzi, Th. Westerwalbesloh, U. Kleineberg, U. Heinzmann, and F. Krausz, Nature (London) **419**, 803 (2002).
[6] H. Mashiko, A. Suda, and K. Midorikawa, Opt. Lett. **29**, 1927 (2004).
[7] N. Miyamoto, M. Kamei, D. Yoshitomi, T. Kanai, T. Sekikawa, T. Nakajima, and S. Watanabe, Phys. Rev. Lett. **93**, 083903 (2004).
[8] J. Andruszkow *et al.*, Phys. Rev. Lett. **85**, 3825 (2000).
[9] H. Wabnitz, L. Bittner, A. R. B. de Castro, R. Döhrmann, P. Gürtler, T. Laarmann, W. Laasch, J. Schulz, A. Swiderski, K. von Haeften, T. Mller, B. Faatz, A. Fateev, J. Feldhaus, C. Gerth, U. Hahn, E. Saldin, E. Schneidmiller, K. Sytchev, K. Tiedtke, R. Treusch, and M. Yurkov, Nature (London) **420**, 482 (2002).
[10] E. Goulielmakis, M. Uiberacker, R. Kienberger, A. Baltuska, V. Yakovlev, A. Scrinzi, Th. Westerwalbesloh, U. Kleineberg, U. Heinzmann, M. Drescher, and F. Krausz, Science **305**, 1267 (2004).
[11] I. Sánchez and F. Martín, Phys. Rev. Lett. **79**, 1654 (1997).
[12] P. Lambropoulos, P. Maragakis, and J. Zhang, Phys. Rep. **305**, 203 (2000).
[13] A. D. Bandrauk, S. Chelkowski, and I. Kawata, Phys. Rev. A **67**, 013407 (2003).
[14] S. Chelkowski, T. Zuo, O. Atabek, and A. D. Bandrauk, Phys. Rev. A **52**, 2977 (1995).
[15] D. Dundas, J. F. McCann, J. Parker, and K. T. Taylor, J. Phys. B **33**, 3261 (2000).
[16] J. Colgan, M. S. Pindzola, and F. Robicheaux, Phys. Rev. A **68**, 063413 (2003).
[17] S. Barmaki, S. Laulan, H. Bachau, and M. Ghalim, J. Phys. B **36**, 817 (2003).
[18] A. Apalategui, A. Saenz, and P. Lambropoulos, J. Phys. B **33**, 2791 (2000).
[19] S. Barmaki, H. Bachau, and M. Ghalim, Phys. Rev. A **69**,

043403 (2004).
[20] A. Palacios, H. Bachau, and F. Martín, J. Phys. B **38**, L99 (2005).
[21] K. Sändig, H. Figger, and T. W. Hänsch, Phys. Rev. Lett. **85**, 4876 (2000).
[22] B. Fabre, J. H. Posthumus, L. Malfaire, E. M. Staicu-Casagrande, J. Jureta, C. Cornaggia, E. Baldit, and X. Urbain, Laser Phys. **14**, 468 (2004).
[23] I. Sánchez and F. Martín, Phys. Rev. Lett. **82**, 3775 (1999).
[24] F. Martín, J. Phys. B **32**, R197 (1999).
[25] D. Charalambidis, D. Xenakis, C. Uiterwaal, P. Maragakis, J. Zhang, H. Schröder, O. Faucher, and P. Lambropoulos, J. Phys. B **30**, 1467 (1997).
[26] H. Bachau, E. Cormier, P. Decleva, J. Hansen, and F. Martín, Rep. Prog. Phys. **64**, 1815 (2001).
[27] M. Cortés and F. Martín, J. Phys. B **27**, 5741 (1994).
[28] I. Sánchez and F. Martín, J. Phys. B **30**, 679 (1997).
[29] E. Cormier and P. Lambropoulos, J. Phys. B **28**, 5043 (1995).
[30] S. Chelkowski, P. B. Corkum, and A. D. Bandrauk, Phys. Rev. Lett. **82**, 3416 (1999).
[31] T.-T. Nguyen-Dang, C. Lefebvre, H. Abou-Rachid, and O. Atabek, Phys. Rev. A **71**, 023403 (2005).